

# The Development of a User Defined Material Model for NiTi SMA Wires

L. Iannucci, P. Robinson and W.L.H. Wan A Hamid

Imperial College London, United Kingdom

## 1 Introduction

Shape memory alloys (SMAs) have attracted enormous attention among researchers since their discovery in 1960s, because of their unique characteristics namely shape memory effect (SME) and Superelasticity or Pseudoelasticity. These characteristics are caused by the change of the SMA crystal structure from a martensite phase to an austenite phase, and vice versa, upon changes in applied temperature or applied mechanical stress. The shape memory effect (SME) has been utilized in various industrial applications including medical, dental, robotics, automotive and aerospace applications. Examples include cylindrical stents to enlarge blood vessels, teeth braces, robotics arms, heat engines, side mirrors of cars, morphing wings and morphing chevrons of jet engines.

Finite element modelling of the SME has been performed by implementing SMA constitutive models into FEA software, ABAQUS. Gao *et al.* [1] developed a one dimensional SMA finite element model by implementing a Brinson constitutive model into a user subroutine in ABAQUS. The model was tested for isobaric, isothermal and constrained recovery cases, and was successively applied to a self-healing hybrid composite to close cracks. However, very little work has been carried out in modelling the shape memory effect (SME) of the SMAs using the commercial explicit FEA software, Ls-Dyna. The most relevant material model in Ls-Dyna is MAT\_030 MAT\_SHAPE\_MEMORY [2], which is ideal for the Superelastic behaviour of the SMAs at a defined constant temperature, but not the SME behaviour with temperature changes.

This paper describes a finite element material model of the shape memory effect (SME) of SMA wires in Ls-Dyna. The SMA wire is modelled as a beam element with one integration point, to mimic the behaviour of a 1-D truss element. One of the earliest one dimensional SMA constitutive model, the Tanaka model [3-4], is implemented within a Ls-Dyna user defined material (UMAT) subroutine, to simulate the thermomechanical behaviour of the SMA wires. The new SMA material model is first validated by comparison with analytical solutions for a SMA wire in series with a spring, before application to a cantilever beam and a more complex corrugated plate structure.

The development of the SMA model in the explicit commercial FEA software, Ls-Dyna, allows modelling of structures in a fast dynamic situation, such as during aircraft actuation. Simulations of potential morphing structures can be made to determine the number of SMA wires, the appropriate SMA cross-sectional area, the structural design or the fiber orientation of composites structures to achieve the intended deformed shapes. The actual deformation of the actuated structures can also be predicted. Moreover, the Ls-Dyna software has a capability of simulating incompressible fluid dynamics (ICFD), which could be used to simulate and analyze the movement of the actuated structures in a realistic air flow condition (fluid-structure interaction - FSI).

## 2 A User Defined Material (UMAT) Model of the SMA

A user defined material (UMAT) model is developed for the shape memory effect (SME) characteristic of NiTi shape memory alloy (SMA) wires. This unique characteristic has frequently been utilized for many applications, such as actuation of morphing structures. Another well-known characteristic of SMA, Superelasticity or Pseudoelasticity, not considered in the current paper. Because the SMA wire acts in one direction, a one-dimensional constitutive model [3-4] was implemented in a user defined subroutine. The SMA wire was modeled as a beam element with one integration point. The truss subroutine was not used because output history variables, *hsv*, cannot be extracted for truss or beam that uses the resultant formulation. The Hughes-Liu beam element formulation (ELFORM = 1) was used for the SMA. The SMA constitutive equation is shown in Eq. 1.

$$\dot{\sigma} = E\dot{\varepsilon} + \Theta\dot{T} + \Omega\dot{\xi} \quad (1)$$

The time-dependant variables  $\dot{\sigma}$ ,  $\dot{\varepsilon}$ ,  $\dot{T}$  and  $\dot{\xi}$  are the stress, strain, temperature and martensite volume fraction of the SMA, respectively.  $E$ ,  $\Theta$  and  $\Omega$  are the modulus of elasticity, thermoelastic coefficient and phase transformation coefficient, respectively. In a total formulation, Eq. 1 is expressed as:

$$\sigma - \sigma_0 = E(\varepsilon - \varepsilon_0) + \Theta(T - T_0) + \Omega(\xi - \xi_0) \quad (2)$$

The thermal expansion part is neglected because the contraction from recovery strain is much higher (1.6% - 4.0%) than the thermal expansion caused by temperature changes (2.6E-05 – 5.5E-05). This is a common assumption in SMA constitutive model development. The modulus of elasticity of the SMA has smaller value in the martensite phase,  $E_M$ , and higher value in the austenite phase,  $E_A$ . The modulus of elasticity is a function of the martensite volume fraction. Meanwhile, the transformation coefficient is a function of the modulus of elasticity. These relations are shown in Eq. 3 and Eq. 4.

$$E(\xi) = E_A - \xi(E_A - E_M) \quad (3)$$

$$\Omega(\xi) = -\varepsilon_L E(\xi) \quad (4)$$

For the Hughes-Liu beam element formulation (ELFORM = 1) in Ls-Dyna, the time step changes with a change in the element length and the wave speed. This wave speed, which is a function of modulus of elasticity and density, changes during the phase transformation of the SMA because the modulus of elasticity changes. Therefore, the time step also changes. The time step and the wave speed are calculated by Eq. 5 and Eq. 6, respectively [5].

$$\Delta t_e = \frac{L}{c} \quad (5)$$

$$c = \sqrt{\frac{E}{\rho}} \quad (6)$$

where  $L$ ,  $c$ ,  $E$ , and  $\rho$  are the element length, the wave speed, the modulus of elasticity and the density, respectively.

The martensite volume fraction for reverse transformation (heating) and martensitic transformation (cooling) are given by Eq. 7 and Eq. 8, respectively.

$$\xi_{M \rightarrow A}(\sigma, T) = e^{a_A(A_s - T) + b_A \sigma} \quad (7)$$

$$\xi_{A \rightarrow M}(\sigma, T) = 1 - e^{a_M(M_s - T) + b_M \sigma} \quad (8)$$

where  $A_s$  and  $M_s$  are austenite and martensite starting temperatures respectively, while  $a_A$ ,  $b_A$ ,  $a_M$  and  $b_M$  are material constants defined by:

$$a_A = \frac{\ln(0.01)}{A_s - A_f}, \quad b_A = \frac{\ln(0.01)}{C_A(A_s - A_f)}, \quad a_M = \frac{\ln(0.01)}{M_s - M_f}, \quad b_M = \frac{\ln(0.01)}{C_A(M_s - M_f)} \quad (9)$$

where  $A_f$  and  $M_f$  are austenite and martensite finishing temperatures respectively. At each time step, Newton Raphson iteration method was applied to solve Eq.2 and Eq. 7/8 using Eq. 10.

$$\sigma_{n+1} = \sigma_n - \frac{f(\sigma_n)}{f'(\sigma_n)} \quad (10)$$

For the reverse transformation (heating), at each time step, Eqs. 2 and 7 were solved iteratively to obtain the stress and martensite volume fraction of the SMA. With initial conditions of zero stress, zero strain and unity martensite volume fraction, the stress function is expressed as:

$$f(\sigma)_{M \rightarrow A} = \sigma - E(\xi)\varepsilon + \varepsilon_L E(\xi)(\xi - 1) \quad (11)$$

First derivative of this function is given by Eq. 12. It is important to note here that the strain,  $\varepsilon$  is treated as a number because it is solved by Ls-Dyna every time the stress of the SMA is obtained. It is also crucial to mention here that the strain is the total strain of the SMA, which is introduced as one of history variables,  $hsv()$ , and not the incremental strain,  $eps(1)$ .

$$f'(\sigma)_{M \rightarrow A} = \frac{\partial f(\sigma)_{M \rightarrow A}}{\partial \sigma} = 1 - \frac{\partial E(\xi)}{\partial \sigma} \varepsilon + \varepsilon_L \left\{ E(\xi) \frac{\partial \xi}{\partial \sigma} + \frac{\partial E(\xi)}{\partial \sigma} (\xi - 1) \right\} \quad (12)$$

Partial differentiation of the martensite volume fraction and the elasticity modulus in Eq. 12 are obtained by differentiating Eq. 7 and Eq. 3 with respect to stress, respectively. These are expressed by Eq. 13 and Eq. 14, respectively.

$$\frac{\partial \xi_{M \rightarrow A}}{\partial \sigma} = b_A e^{a_A(A_s - T) + b_A \sigma} = b_A \xi_{M \rightarrow A} \quad (13)$$

$$\frac{\partial E(\xi)}{\partial \sigma} = (E_M - E_A) \frac{\partial \xi_{M \rightarrow A}}{\partial \sigma} = (E_M - E_A) b_A \xi_{M \rightarrow A} \quad (14)$$

Material Constants	SMA material properties / variables	Values
-	Mass density, $\rho$	7.89E-06 kg/mm <sup>3</sup>
cm(1)	Elastic modulus at martensite phase, $E_M$	40 GPa
cm(2)	Poisson's ration, $\nu$	0.3
cm(3)	Elastic modulus at austenite phase, $E_A$	75 GPa
cm(4)	Martensite starting temperature, $M_s$	47 °C
cm(5)	Martensite finishing temperature, $M_f$	43 °C
cm(6)	Austenite starting temperature, $A_s$	60 °C
cm(7)	Austenite finishing temperature, $A_f$	65 °C
cm(8)	Stress influenced coefficient at martensite phase, $C_M$	0.0082 Gpa/°C
cm(9)	Stress influenced coefficient at austenite phase, $C_A$	0.0082 Gpa/°C
cm(10)	Maximum recoverable strain, $\varepsilon_L$	0.016
cm(11)	Diameter of SMA wire, $\emptyset$	0.1/0.2/0.5 mm
cm(12)	Length of SMA wires (early stage of model developement), $l$	-
cm(13)	Stiffness of linear spring (early stage of model developement), $k$	-
cm(14)	Maximum number of iteration (convergence criteria), $n_{max}$	500
cm(16)	Bulk modulus, $B$	33.33 GPa
cm(17)	Shear modulus, $G$	15.38 GPa
cm(18)	FEA simulation case: 1. A spring-SMA case (actuated structure) 2. A constant load case	1 or 2
cm(19)	Relaxation time (for constant load case), $t_{relaxation}$	10,000 ms
cm(20)	Monitoring: 0. Switch off print statements 1. Switch on print statements	0 or 1

Table 1: UMAT material constants and material properties of SMA wire.

For the martensitic transformation (cooling), Eqs. 2 and 8 were solved iteratively at each time step, to obtain the stress and martensite volume fraction of the SMA. With initial conditions of zero martensite volume fraction, non-zero initial stress and strain which were obtained from the final values at the end of previous heating, the stress function is expressed as:

$$f(\sigma)_{A \rightarrow M} = \sigma - \sigma_0 - E(\xi)(\varepsilon - \varepsilon_0) + \varepsilon_L E(\xi) \xi \quad (15)$$

This function differentiated with respect to stress gives:

$$f'(\sigma)_{A \rightarrow M} = \frac{\partial f(\sigma)_{A \rightarrow M}}{\partial \sigma} = 1 - \frac{\partial E(\xi)}{\partial \sigma} (\varepsilon - \varepsilon_0) + \varepsilon_L \left\{ E(\xi) \frac{\partial \xi}{\partial \sigma} + \xi \frac{\partial E(\xi)}{\partial \sigma} \right\} \quad (16)$$

Partial differentiation of the martensite volume fraction and the elasticity modulus in Eq. 16 are obtained by differentiating Eq. 8 and Eq. 3 with respect to stress, and expressed by Eq. 17 and Eq. 18, respectively.

$$\frac{\partial \xi_{A \rightarrow M}}{\partial \sigma} = -b_M e^{a_M(M_s - T) + b_M \sigma} = b_M (\xi_{A \rightarrow M} - 1) \quad (17)$$

$$\frac{\partial E(\xi)}{\partial \sigma} = (E_M - E_A) \frac{\partial \xi_{A \rightarrow M}}{\partial \sigma} = (E_M - E_A) b_M (\xi_{A \rightarrow M} - 1) \quad (18)$$

All equations were introduced as history variables within the UMAT subroutine, with Eq. 7 and Eqs. 11-14 in a heating loop, while Eq. 8 and Eqs. 15-18 in a cooling loop. Eq. 10 was used in both loops to calculate the stress of the SMA for each time increment. The material properties of the SMA wire were obtained from the manufacturer datasheet, SAES [6], and were assigned to the material model through material constants in the UMAT keyword deck. These are listed in Table 1. The SMA material model is first tested for a case of a SMA wire connected to a linear spring in series, which is validated by analytical solution presented in the next section 3. The modelling approach is applied to a cantilever beam, and finally to a pre-curved corrugated plate. A vectorized UMAT has been developed for the pre-curved corrugated plate actuated by multiple SMA wires. This increases the simulation speed as all beam elements of the SMA are processed simultaneously at each time step.

### 3 Analytical Formulation

To validate the SMA material model implementation, analytical solutions for the SMA wire connected to a linear spring in series were solved in MATLAB. One complete heating-cooling cycle was applied on the SMA wire, and the stress was calculated iteratively using Eq. 10. In contrast to the FEA model, the analytical strain was treated as a variable which is a function of the SMA stress, as expressed in Eq. 19. For the iteration, the stress functions and their derivatives of the martensite-to-austenite transformation (heating) and the austenite-to-martensite transformation (cooling) are given by Eqs. 20-21 and Eqs. 22-23, respectively. The respective partial derivatives of the martensite volume fraction and the stiffness are similarly defined in the previous Eqs. 13-14 and Eqs. 17-18.

$$\varepsilon = \frac{\Delta l}{l} = -\frac{F}{kl} = -\frac{\sigma A}{kl} \quad (19)$$

$$f(\sigma)_{M \rightarrow A} = \sigma + E(\xi) \frac{\sigma A}{kl} + \varepsilon_L E(\xi) (\xi - 1) \quad (20)$$

$$f'(\sigma)_{M \rightarrow A} = \frac{\partial f(\sigma)_{M \rightarrow A}}{\partial \sigma} = 1 + \frac{A}{kl} \left\{ E(\xi) + \sigma \frac{\partial E(\xi)}{\partial \sigma} \right\} + \varepsilon_L \left\{ E(\xi) \frac{\partial \xi}{\partial \sigma} + \frac{\partial E(\xi)}{\partial \sigma} (\xi - 1) \right\} \quad (21)$$

$$f(\sigma)_{A \rightarrow M} = \sigma - \sigma_0 + E(\xi) \left( \frac{\sigma A}{kl} + \varepsilon_0 \right) + \varepsilon_L E(\xi) \xi \quad (22)$$

$$f'(\sigma)_{A \rightarrow M} = \frac{\partial f(\sigma)_{A \rightarrow M}}{\partial \sigma} = 1 + \frac{A}{kl} \left\{ E(\xi) + \sigma \frac{\partial E(\xi)}{\partial \sigma} \right\} + \varepsilon_0 \frac{\partial E(\xi)}{\partial \sigma} + \varepsilon_L \left\{ E(\xi) \frac{\partial \xi}{\partial \sigma} + \xi \frac{\partial E(\xi)}{\partial \sigma} \right\} \quad (23)$$

For the cantilever beam, it is well known that the tip deflection is given by:

$$\delta_{tip} = \frac{FL^3}{3EI} \quad (24)$$

Hence to validate the SMA stress and strain for the cantilever beam case, the analytical SMA-spring model was solved in MATLAB by replacing the stiffness ( $k$ ) value with the stiffness calculated by Eq. 25.

$$\frac{F}{\delta_{tip}} = \frac{3EI}{L^3} \quad (25)$$

## 4 FEA Simulation Results

The FEA simulation results of the user defined material (UMAT) model for the SMA wire are presented in the following sections. The material model was initially validated prior to detailed actuator simulations of a cantilever beam and a pre-curved corrugated plate. Several cases are presented for the pre-curved corrugated plate, such as the number of SMA wires per cell and the configuration of SMA wires in each cell.

### 4.1 Validation of SMA Material Model

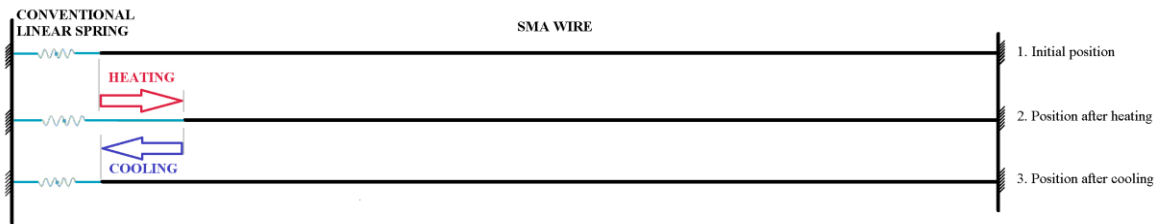


Fig. 1: A SMA wire connected to a linear spring in series.

The UMAT was initially validated by an analytical solution as described in section 3. For a SMA wire connected to a linear spring in series (Fig.1), the linear spring was modelled as a discrete element with a spring stiffness of 3.5 N/mm, while the SMA wire was modelled as a beam element with one integration point (QR/IRID = 1). The Hughes-Liu beam element formulation (ELFORM = 1) with a circular/tubular cross section (CST = 1) was applied. The inner (TT1 and TT2) and outer (TS1 and TS2) diameter of the cross section were defined as 0 mm and 0.5 mm, respectively. One end of the SMA wire and the spring were fixed in all degree of freedoms, and one complete heating-cooling cycle was applied on the SMA wire.

Figure 2 shows the stresses and strains in the SMA, respectively. The solid lines represent the FEA simulation results while the dotted lines represent the analytical solutions. As the temperature increases above austenite starting temperature  $A_s$ , the SMA wire contracts (the strain decreases) and extends the linear spring, hence the SMA stress increases. These are shown by the red lines. After this actuation, the temperature decreases and consequently reduces the stiffness of the SMA wire from  $E_A$  to  $E_M$ . As a result, the linear spring extends the SMA wire, hence the SMA strain increases and the SMA stress decreases, as shown in blue. The results show excellent agreement between analytical and numerical solutions.

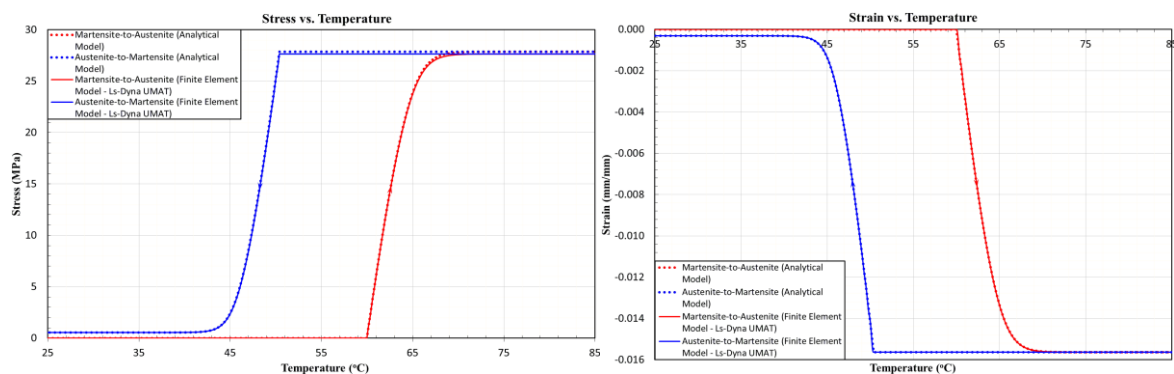


Fig.2: Validation of SMA stress and strain by analytical solutions.

This model was run on a computer with 8 CPUs and 32 GB memory capacity, and was solved in 31 minutes (CPU time). In a preliminary check, the kinetic energy of the SMA wire increased slightly at the beginning of heating, by approximately 4.5  $\mu$ J, and then decreased back until zero at the end of heating. The kinetic energy slightly increased again at the start of cooling, by approximately 4.9  $\mu$ J, and drops to zero at the end of cooling. This assured that the SMA wire reached equilibrium state at the end of heating and cooling cycles. The SMA internal energy decreased by approximately 4.25 mJ

during heating, then maintained at a constant value once the martensite-to-austenite transformation completed, and then increased back during cooling. An opposite trend was observed for the internal energy of the linear spring. This showed that the loss of the SMA internal energy due to work done on the linear spring during heating (actuation), was converted to potential energy, stored in the linear spring. This stored potential energy was used to retract the SMA wire during cooling. The hourglass energy be zero at all time, which ensured that there were no hourglass problems in the SMA material model.

#### 4.2 A Cantilever Beam Actuated by a SMA Wire

The previous section showed the interaction between the SMA wire and the discrete element, a linear spring. Before applying the SMA wire on a more complex structure, a cantilever beam actuated by the SMA wire was modelled in Ls-Dyna to show the interaction between the SMA material model and shell elements. The SMA wire has a diameter of 0.5 mm, a length of 100 mm, and a maximum recoverable strain of 1.6%. The aluminium cantilever beam was modelled with shell elements with a density of 2.81E-06 kg/mm<sup>3</sup>, a Young's modulus of 71.7 GPa and a flexural stiffness (EI) of 5975 kNmm<sup>2</sup>. The length, width and height of the cantilever beam were 225 mm, 1 mm and 10 mm, respectively. One end of the cantilever beam was fixed in all degree of freedoms while the other end was free and was actuated by the SMA wire in a vertical direction, as shown in Fig. 3a. One complete heating-cooling cycle was applied to the SMA wire.

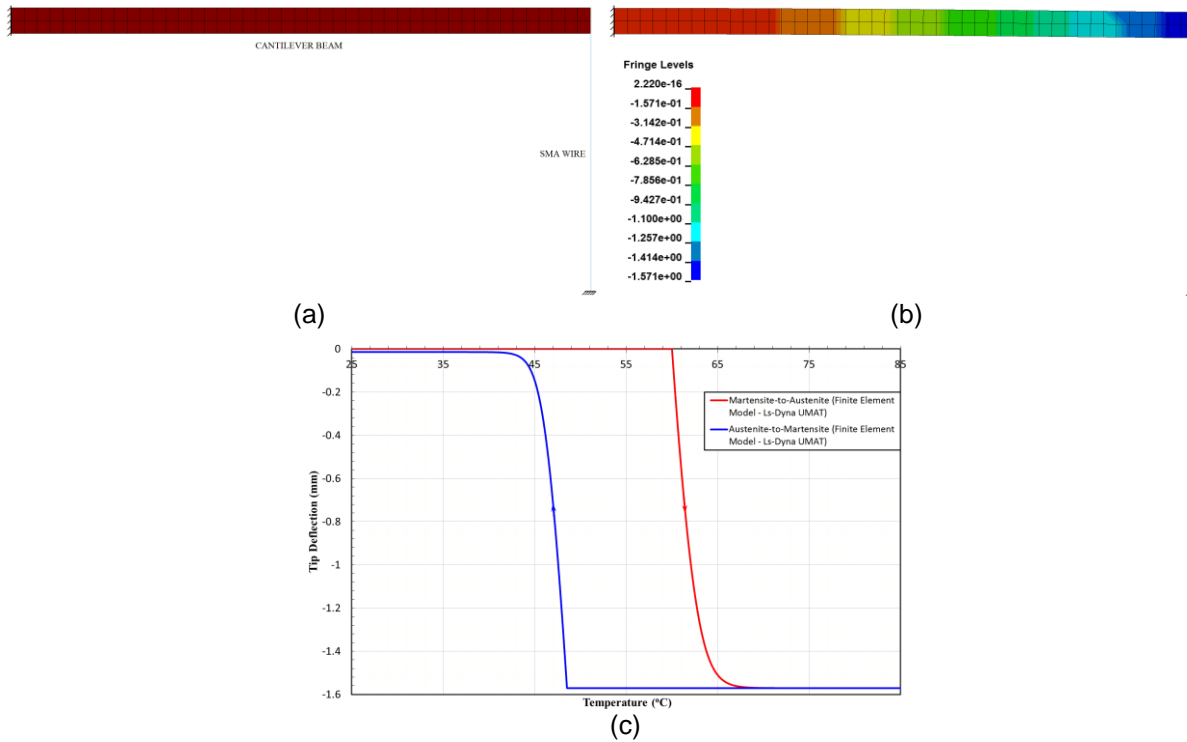


Fig.3: A cantilever beam (a) before and (b) after actuation, (c) tip deflection of the cantilever beam.

The actuation of this cantilever beam model was run on a computer with 4 CPUs and 32 GB memory capacity, and was completed in 1 hour and 50 minutes (CPU time). The deformation of the cantilever beam after SMA actuation is shown in Fig. 3b. The resulted vertical tip deflection of the cantilever beam is 1.57 mm, as shown by the fringe levels. The tip deflection as a function of temperature is shown in Fig. 3c. The stress developed in the SMA wire and the SMA strain for one complete heating-cooling cycle are depicted in Fig. 4a and 4b, respectively. They show excellent agreement with analytical solutions, which were solved in MATLAB with spring stiffness ( $F / \delta$ ) of 1.5737 N/mm. The recovery stress after the completion of the heating cycle is smaller (around 12.6 MPa) compared to the previous example, because the stiffness in the actuation direction is smaller. In contrast, the recovery strain achieved at the end of the heating cycle is slightly higher in magnitude (1.58%), which is close to the maximum recoverable strain of the SMA wire (1.6%).

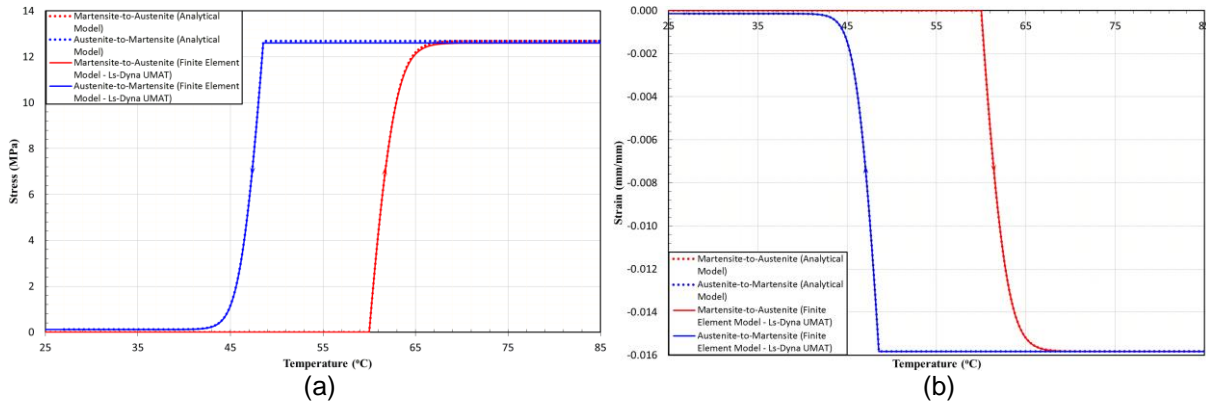


Fig.4: (a) Stress and strain of the SMA wire for the actuation of the cantilever beam.

### 4.3 Pre-curved Corrugated Plates

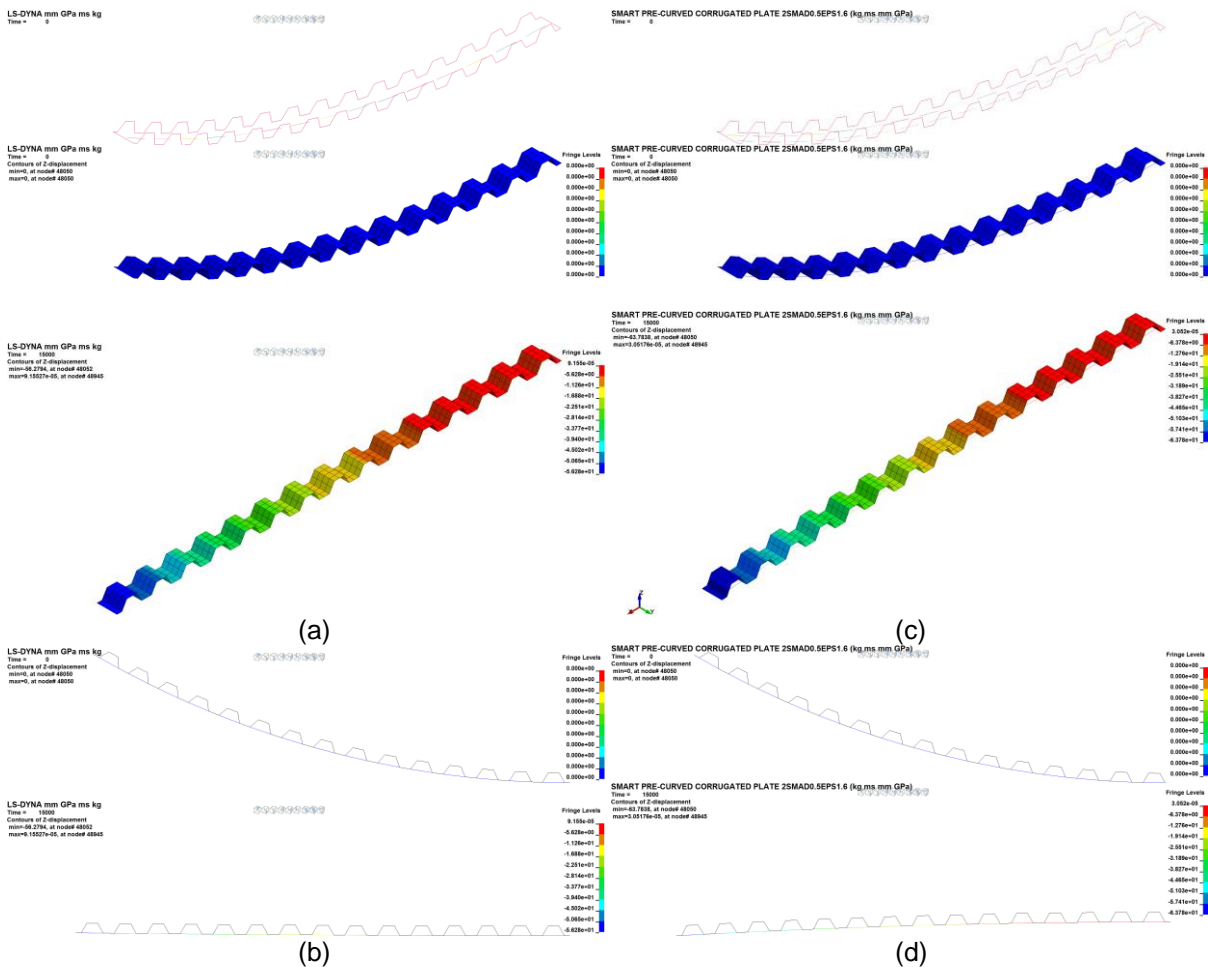


Fig.5: Pre-curved corrugated aluminium plates actuated by one SMA wire per cell: (a) isometric view and (b) side view, and by two SMA wires per cell: (c) isometric view and (d) side view.

To demonstrate the applicability of the developed SMA material model on a more complex structure, the model was further tested for actuation of pre-curved corrugated plates. The plates were modelled with shell elements, with a plate width of 10 mm, a length of 225 mm, a thickness of 1 mm, and 15 cells. The corrugated plates were modelled using aluminium material with material properties similar to the previous cantilever beam. The SMA wires have a diameter of 0.5 mm, with material properties listed in Table 1. A Fixed boundary condition in all degree of freedoms was applied on one end of the plates while the other end was free. A symmetrical boundary condition was applied on the side edges of the plates. One complete heating-cooling cycle was applied on the SMA wires, and the vertical tip

deflection of the free end was evaluated. Two cases are presented for the actuation of the pre-curved corrugated plates. Firstly, each cell was actuated by one SMA wire and two SMA wires, to investigate the effect of increasing the number of SMA wires per cell. Secondly, the configurations or arrangements of the SMA wires in the cells were varied to study their effect on the tip deflection.

Fig. 5 shows simulation results of the pre-curved corrugated aluminium plate actuated by one SMA wire per cell (5a) and two SMA wires per cell (5c). The former was run on a computer with 4 CPU and 32 GB memory capacity, while the later was run on the High Performance Computer (HPC) of Imperial College London with 24 CPUs and 20 GB memory capacity. They were completed in 603 hours and 39 minutes (elapsed time), and 46 hours and 28 minutes (elapsed time), respectively. The simulation on HPC was completed about 13 times faster than the simulation on the normal computer, because of higher number of CPUs. The resulted vertical tip deflections due to the SMA wires actuation are 56.3 mm and 63.8 mm, respectively. It shows that increasing the number of the SMA wires by two (hence increase in power requirement) increases the tip deflection by only 13.3%.

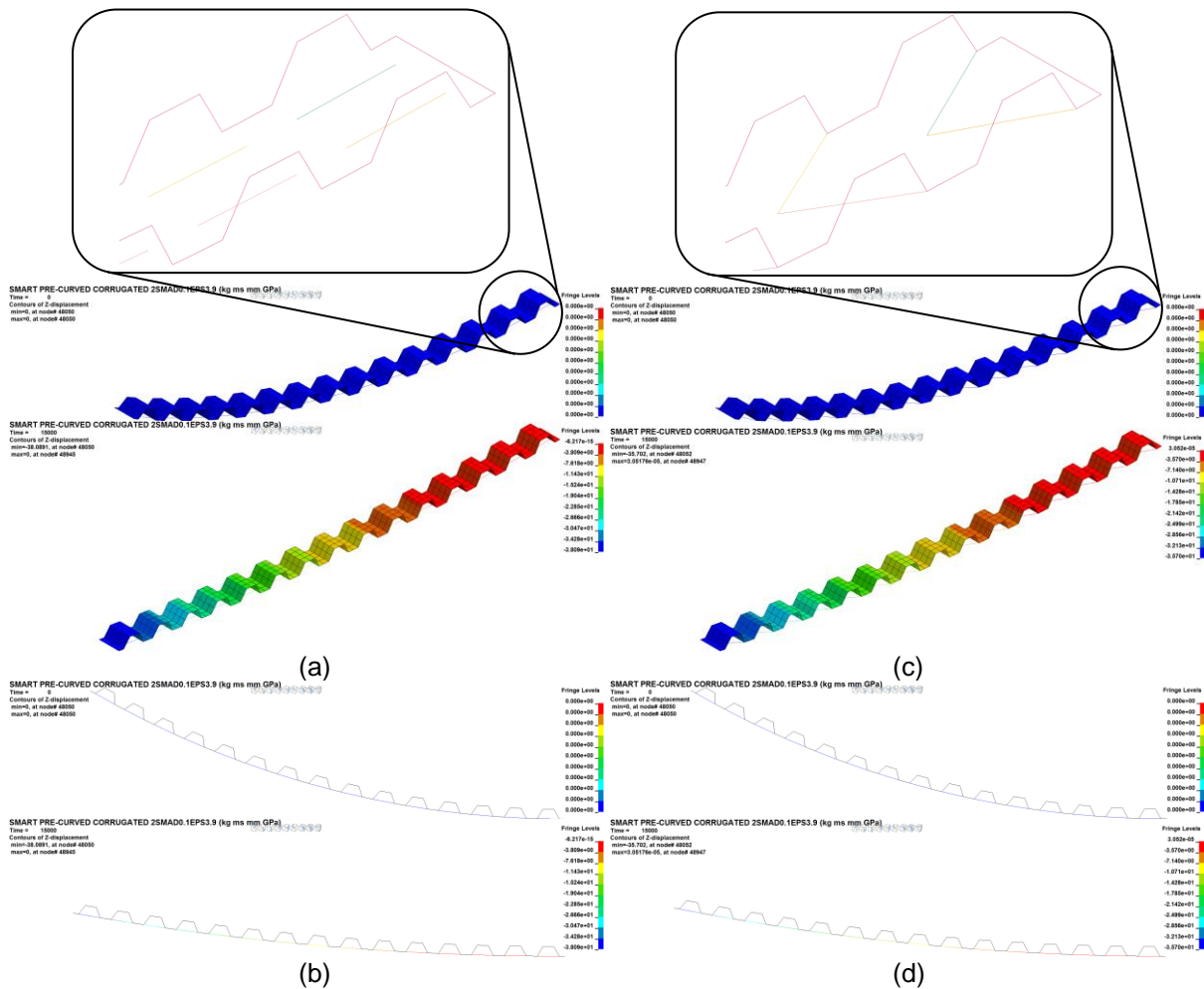


Fig.6: Pre-curved corrugated aluminium plates actuated by 2 SMA wires per cell in parallel: (a) isometric view and (b) side view, and by 2 SMA wires per cell in 'V' configuration: (c) isometric view and (d) side view.

In addition to the analysis of the number of SMA wires per cell, their configurations or arrangements were also varied. Two SMA wires in each cell were arranged in parallel and 'V' configurations, as depicted in Fig. 6a and 6c, respectively. In this analysis, SMA wires with a diameter of 0.1 mm and a maximum recoverable strain of 3.9% were used. This was intentionally performed to allow the parallel configuration to be compared with the previous pre-curved corrugated plate actuated by SMA wires having a larger diameter, but a smaller maximum recoverable strain (Fig. 5c and 5d). The simulation results show maximum vertical tip deflections of 38.1 mm and 35.7 mm for the parallel and 'V' configurations, respectively. Therefore, the SMA wires with the parallel configuration are preferable because a slightly larger tip deflection can be achieved. However, the maximum tip deflection (38.1 mm) for the parallel configuration is much smaller than the maximum tip deflection achieved by the

pre-curved corrugated plate actuated by SMA wires having 0.5 mm diameter and 1.6% maximum recoverable strain shown in the previous Fig. 5c and 5d (63.8 mm). This shows that the influence of the SMA cross-sectional area on the tip deflection of the pre-curved corrugated plate is greater than the influence of the maximum recoverable strain.

## 5 Conclusions and Future Work

A SMA material model has been successfully implemented in Ls-Dyna and verified with analytical solutions. The model was then tested for actuation of a cantilever beam, which was also validated, before application on a pre-curved corrugated plate. From actuation of the pre-curved corrugated plates, it can be concluded that increasing the number of SMA wires per cell for a large diameter SMA wire (0.5 mm) resulted in a small increase in the tip deflection. A parallel configuration of SMA wires in each cell gives slightly higher tip deflection compared to a 'V' configuration. The SMA model development, verification, and trials in the explicit commercial FEA software, Ls-Dyna, has allowed the possibility of modelling a wing design in a fast dynamic situation, such as flight control actuation. It could also be employed in other fields that involves dynamic situation, such as structural impact. The next step in this work is to apply the SMA material model to actuate a morphing wing with flight aerodynamic pressure acting on the wing. In addition to that, the SMA wires under cyclic thermal loading is another important aspect to be investigated.

## 6 Summary

A user defined material (UMAT) model for shape memory alloy (SMA) wires has been developed and implemented into the explicit finite element analysis software, Ls-Dyna. The validation of the thermomechanical behaviour of the SMA material model by analytical solutions shows excellent agreement. The SMA material model has been validated against the actuation of a cantilever beam, and finally applied to the actuation of a pre-curved corrugated plate. For the cantilever beam, a very small tip deflection was achieved, approximately 1.57 mm, when actuated perpendicularly by a SMA wire with a length of 100 mm. The actuation of the pre-curved corrugated plates shows the amplification of the tip deflection when actuated by SMA wires in each cell, compared to the actuation of the cantilever beam. Increasing the number of SMA wires per cell is not preferable for a large diameter SMA wires (e.g. 0.5 mm), due to the small increment in the tip deflection. If two or more SMA wires are used in each cell, a parallel configuration gives slightly higher tip deflection compared to a 'V' configuration. The simulation speed of the pre-curved corrugated plates has been greatly increased by developing a vectorized UMAT for the SMA material model. The completion of this research provides a firm foundation for future exploration of structures actuated by SMA wires. The developed UMAT for the SMA wire can be used as a design tool to virtually design realistic composite morphing wings. It permits a design of structures under fast dynamic condition because the model has been developed within the explicit FEA software, Ls-Dyna. The model allows the prediction of the number of the SMA wires and also the appropriate SMA diameter or cross-sectional area to achieve the targeted configuration. A realistic structural design, an optimum fiber orientation of composites, and actual deformation of the actuated structures can also be predicted. The capability of the commercial Ls-Dyna software to perform optimization tasks using LS-OPT and to simulate an incompressible fluid dynamics (ICFD) simulation, can be utilized in a future research to optimize the structural design and to analyze the fluid-structure interaction (FSI) between the movement of actuated surfaces and a fluid flow.

## 7 Literature

- [1] Gao, X, Qiao, R and Brinson, L C: "Smart Materials and Structures", 16, 2007, 2102-2115.
- [2] Livermore Software Technology Corporation (LSTC): "LS-DYNA Version R8.0 Keyword User's Manual", Volume II, 2015.
- [3] Tanaka, K, Hayashi, T and Itoh, Y: "Mechanics of Materials", 13, 1992, 207-215.
- [4] Tanaka, K, Kobayashi, S and Sato, Y: "International Journal of Plasticity", 2, 1986, 59-72.
- [5] Livermore Software Technology Corporation (LSTC): "LS-DYNA Theory Manual", 2016.
- [6] S.A.E.S. Group (Societa Apparecchi Elettrici Scientifici – Electrical and scientific components company): "SmartFlex wire and springs datasheet", 2009.